

## Dynamical simulation of the Interstellar Comet 3I/ATLAS

GOLDY AHUJA  <sup>1,2</sup> AND SHASHIKIRAN GANESH  <sup>1</sup><sup>1</sup>Physical Research Laboratory, Ahmedabad, Gujarat-380009, India<sup>2</sup>Indian Institute of Technology Gandhinagar, Palaj, Gujarat-382355, India

Submitted to ApJL

## ABSTRACT

Comet 3I/ATLAS, also known as C/2025 N1, was discovered on 2025 July 1 UT by NASA Asteroid Terrestrial-impact Last Alert System (ATLAS), with a  $v_\infty \sim 58 \text{ km s}^{-1}$ . This is the fastest among the three interstellar objects discovered so far. In this work, we study the interaction of the 3I/ATLAS with Mars, pre-perihelion, and Jupiter post-perihelion. We also present the results of the dynamical simulations of the orbital evolution of the comet for a hundred years in the past and future. For our analysis, we have used REBOUND, an N-Body simulation package, to study these situations. We use the adaptive size mathematical integrator IAS15, with a 1-day time step for long-term integration, and a 1-hour time step to study the effect of the planets on this body during the close encounters. We have seen an effect of Jupiter on the orbital parameters of the comet, which affects its post-perijove trajectory significantly. The impact of Mars on this comet is minimal compared to the effect of Jupiter. This is consistent with the point that the comet moves well past Mars's Hill radius but very close to Jupiter's Hill radius at the respective close approaches. However, the effect of non-gravitational forces will alter the results. Since the non-gravitational forces are not yet known, we predict the variation of the orbital parameters considering a range of possible magnitudes of the non-gravitational acceleration.

*Keywords:* Comets (280) — Interstellar Objects (52) — Comet dynamics (2213) – N-body simulations (1083)

## 1. INTRODUCTION

Interstellar comets are small bodies that are formed outside our solar system and are found passing through the Solar system. They are expected to have been formed in a protoplanetary disk and then thrown out of the parent star system, possibly due to gravitational scattering by heavy bodies, such as planets, present in the disk (D. Jewitt & D. Z. Seligman 2023). They travel through the ISM before encountering any other stellar system, such as the solar system. Two interstellar visitors have been recorded passing through the solar system. The first one was 1I/'Oumuamua or C/2017 U1, a metallic asteroid-like object with no visible coma (K. J. Meech et al. 2017; Q.-Z. Ye et al. 2017; 'Oumuamua ISSI Team et al. 2019). The second one was the comet 2I/Borisov or C/2019 Q4, well studied by many authors (C. Opitom et al. 2019; A. Fitzsimmons et al. 2019; D. Jewitt et al. 2020; P. Guzik et al. 2020; D. Bodewits

et al. 2020; K. Aravind et al. 2021; G. P. Prodan et al. 2024). Recently, the third interstellar object, 3I/ATLAS or C/2025 N1, hereafter 3I, has been discovered at a heliocentric distance of 4.51 au, with an eccentricity of  $6.13 \pm 0.02$  (B. T. Bolin et al. 2025; D. Z. Seligman et al. 2025). The comet is moving with a very high radial velocity of around  $58 \text{ km s}^{-1}$  and was at a perihelion distance of  $1.357 \pm 0.001$  au in October 2025.

The interstellar comet 3I made a close approach to Mars at a distance of 0.194 au on Epoch JD 2460951.5 (2025 October 03)<sup>3</sup> and will be approaching Jupiter at a distance of 0.357 au on Epoch JD 2461115.5 (2026 March 16)<sup>4</sup>. The interaction of the comet with Mars and Jupiter is shown in the figure 1. At those distances from the respective planets, the comet's orbital elements will be affected due to gravitational perturbation from these planets, resulting in a change in trajectory.

<sup>3</sup> HORIZONS ephemeris for interaction with Mars<sup>4</sup> NASA SBDB lookup showing close approach with Jupiter

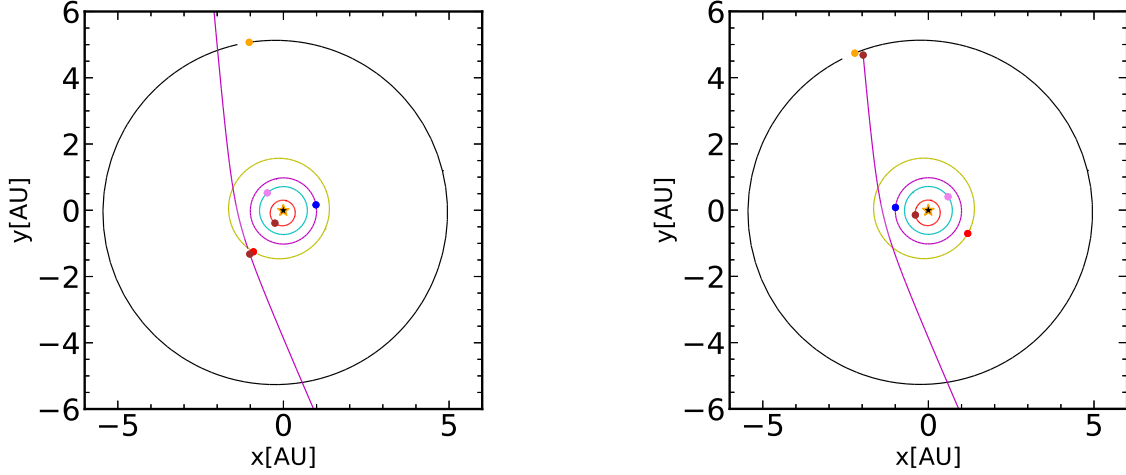


**Figure 1.** Left: Close encounters between interstellar comet 3I/ATLAS with Mars at Epoch JD 2460951.5 (2025 October 03). Right: Close encounters between interstellar comet 3I/ATLAS with Jupiter at Epoch JD 2461115.5 (2026 March 16). For clarity, we show only the planets' orbits (up to Jupiter), whereas, in the simulation, we have also considered the three other planets (Saturn, Uranus, Neptune), the four big asteroids (Ceres, Pallas, Juno, Vesta) in the asteroid belt, and five KBOs (Pluto, Makemake, Haumea, Quaoar, Sedna).

Alongside the gravitational perturbations, comets are also subject to non-gravitational forces due to the sublimation of volatile ices, which exerts a recoil acceleration on the comet's nucleus, affecting their orbital evolution (B. G. Marsden et al. 1973; M.-T. Hui & D. Jewitt 2017). For example, both the previously seen interstellar objects have been subjected to non-gravitational forces (M. Micheli et al. 2018; D. Jewitt & D. Z. Seligman 2023).

The evolution of a comet's orbit is studied numerically using dynamical N-body simulation codes. Such dynamical simulations (C. de la Fuente Marcos & R. de la Fuente Marcos 2012; M. Królikowska & P. A. Dybczyński 2010; P. A. Dybczyński & M. Królikowska 2011; C. de la Fuente Marcos & R. de la Fuente Marcos 2014; R. Gabryszecki et al. 2024) have become a viable option in recent years to study the long-term effects of gravitational and non-gravitational forces and to examine any close encounters with the planets (P. M. Shober et al. 2024; S. Anderson et al. 2024; S. Pilorz & P. Jenniskens 2025).

In this letter, we discuss the dynamics of interstellar comet 3I at different timescales. We start our discussion with the past (and future) dynamical trajectory by integrating backwards (and forwards) for timescales of 100 years, with a timestep of 1 day. We study the effect of the interactions with Mars and Jupiter at a timestep of 1 hour and limit our simulation to a 20-year period (at which point the comet reaches close to 250 au - just outside the planetary perturbation limits (M. Królikowska & P. A. Dybczyński 2010; P. A. Dybczyński & M. Królikowska 2011)).

In section 2, we discuss the methodology followed to set up the dynamical simulations and compute the interaction of comet 3I with Mars and Jupiter. In section 3, we show the past and future orbital evolution of this comet for 100 years under the effect of gravitational perturbation. We also study the effect of the interactions with Mars and Jupiter by considering two different simulations - one with both planets and one in their absence. In section 3.2.3, we assume a range of non-gravitational accelerations that the comet may be subjected to, and predict the variation of the orbital parameters under the effect of both gravitational and non-gravitational forces.

## 2. METHODOLOGY

To understand comet 3I's long-term past and future dynamical behavior, we have used the PYTHON-based REBOUND N-body simulation package (H. Rein & S. F. Liu 2012). We have used different integrators to solve for the two timescales as discussed below. For long-term integrations in the past and future to see the projection of the comet, and to study the interaction with planets such as Mars and Jupiter, we have used the non-symplectic mathematical integrator, i.e., Integrator with Adaptive Step-size control, 15th order (IAS15), which is very accurate up to machine precision (H. Rein & D. S. Spiegel 2015). For long-term integration, the time step of 1 day is chosen, and for the planetary interaction, we have considered 1 hour to be optimal to study changes in the different orbital parameters and the comet's Cartesian velocities.

**Table 1.** Heliocentric and Barycentric Orbital Elements of Interstellar comet 3I/ATLAS.

Orbital Parameters	Units	Heliocentric	Barycentric
Perihelion Distance (q)	au	$1.3572 \pm 0.0006$	1.3626
Semi-major axis (a)	au	$-0.2638 \pm 0.0001$	-0.2642
Eccentricity (e)	–	$6.145 \pm 0.004$	6.157
Inclination (i)	degree	$175.1135 \pm 0.0003$	175.1275
Longitude of Ascending Node ( $\Omega$ )	degree	$322.166 \pm 0.006$	322.255
Argument of Perihelion ( $\omega$ )	degree	$128.004 \pm 0.005$	128.083

NOTE—The Epoch of these elements is JD 2460867.5 (2025-07-11 00:00:00). The results are based on 601 observations used, which covers the data span of 58 days<sup>5</sup>.

We make use of the NASA JPL’s Small Body Database lookup (SBDB)<sup>5</sup> and JPL Horizons service<sup>6</sup>(J. D. Giorgini et al. 1996) to get the orbital elements and covariance matrices of the orbital elements of the comet 3I at Epoch JD 2460867.5 (2025 July 11, 00:00:00 UT). The Heliocentric orbital elements with  $1-\sigma$  uncertainties and the corresponding Barycentric orbital elements of comet 3I are given in Table 1. After getting the covariance matrix, we followed the approach of A. Egal et al. (2022); S. E. Anderson et al. (2023) to create 500 massless clones of the interstellar comet 3I using the multivariate distribution.

The orbits of the statistical clones are numerically integrated in the presence of the eight major planets, four of the large asteroids present in the asteroid belt, i.e, Ceres, Pallas, Juno, and Vesta, and the five big KBOs, namely, Pluto, Makemake, Haumea, Quaoar, and Sedna. We consider the barycenter of the planets at a similar epoch to the comet 3I in the simulation. The values and the error bars of the different quantities, reported in the text, are calculated by taking the mean and the standard deviation of the values of the parameters for all 500 clones.

### 3. RESULTS AND DISCUSSION

In this section, we discuss the results of the dynamical simulation of both the past and future orbital integrations of the comet 3I’s nominal orbit and the statistical clones.

#### 3.1. Past Evolution

We evolved the orbit of 3I for a hundred years into the past and found the comet to be at a distance of  $1228.58 \pm 0.23$  au, originating from the Sagittarius constellation with a geocentric coordinate RA ( $\alpha$ ) and Declination ( $\delta$ ) of  $294.9691^\circ \pm 0.0041^\circ$ , and  $-19.0766^\circ \pm 0.0007^\circ$  respectively. The comet is approaching with a radial velocity of  $-57.995 \pm 0.011$  kms $^{-1}$ . We have used the ASTROPY package to convert the equatorial coordinates into Galactic coordinates and Ecliptic coordinates. The Galactic longitude,  $l$ , is found to be  $20.6913^\circ \pm 0.0022^\circ$  and the Galactic latitude is  $-18.9947^\circ \pm 0.0033^\circ$ . The Ecliptic longitude ( $\lambda$ ) is  $293.530^\circ \pm 0.004^\circ$ , and the Ecliptic latitude ( $\beta$ ) is  $2.3459^\circ \pm 0.0001^\circ$ .

The velocities in the ICRS frame,  $v_x$ ,  $v_y$  and  $v_z$ , are found to be  $-23.198 \pm 0.008$ ,  $49.647 \pm 0.008$  kms $^{-1}$  and  $18.943 \pm 0.003$  kms $^{-1}$ . The Cartesian velocities are converted into Galactic space velocities using the method given in D. R. H. Johnson & D. R. Soderblom (1987), where the transformation matrix has been updated at the epoch J2000. The Galactic space velocities ( $U$ ,  $V$ ,  $W$ ) are  $-51.26 \pm 0.01$ ,  $-19.40 \pm 0.01$ ,  $18.93 \pm 0.01$  kms $^{-1}$ . Here, we have used the galactocentric sign convention that  $U$  is negative in the direction of the Galactic center,  $V$  is positive in the direction of Galactic rotation, and  $W$  is positive in the direction of the North Galactic Pole (NGP). These velocities have been corrected for the mean solar motion velocities ( $U$ ,  $V$ ,  $W$ ) $_{\odot} = (11.1, 12.24, 7.25)$  kms $^{-1}$  with respect to the local standard of rest (LSR) (R. Schönrich et al. 2010). The corrected velocities of the comet 3I are  $(62.36 \pm 0.69, -7.16 \pm 0.47, 26.18 \pm 0.36)$  kms $^{-1}$ . These results closely match those reported by R. de la Fuente Marcos et al. (2025).

R. de la Fuente Marcos et al. (2025) argue that the comet is originating from the thin disk as the

<sup>5</sup> [https://ssd.jpl.nasa.gov/tools/sbdb\\_lookup.html#/?sstr=3I%20FATLAS](https://ssd.jpl.nasa.gov/tools/sbdb_lookup.html#/?sstr=3I%20FATLAS)

<sup>6</sup> <https://ssd.jpl.nasa.gov/horizons/>

$(U_{LSR}^2 + W_{LSR}^2)^{1/2}$  is less than 85  $\text{km s}^{-1}$  (based on Fig 3 of T. Bensby et al. (2003)). However, Fig 7 in M. P. da Silva et al. (2023) shows that the  $V_{Total} = (U_{LSR}^2 + V_{LSR}^2 + W_{LSR}^2)^{1/2}$  range between 50  $\text{km s}^{-1}$  and 70  $\text{km s}^{-1}$  is characterized as the probable zone of the transition between the thin and thick disk components. For Comet 3I, the corresponding  $V_{Total} = 68.01 \pm 0.82 \text{ km s}^{-1}$ . Therefore, we believe that the place of origin of comet 3I is uncertain. This is consistent with the conclusion by M. J. Hopkins et al. (2025). Further spectroscopic estimation of metallicity for this comet will help to define its place of origin among the thin or thick disk.

### 3.2. Future Evolution

We have divided this subsection into two parts. In the first part, we discuss the long-term future integration of 100 years with the IAS15 integrator with a time step of 1 day. In the second part, we have performed a precise simulation of 20 years with a time step of 1 hour using the IAS15 integrator.

#### 3.2.1. Long-term integration

During the long-term integration, we have simulated the integration of comet 3I and its clones over a period of 100 years. The projected RA ( $\alpha$ ) and Declination ( $\delta$ ) of the comet after 100 years are found to be  $95.321^\circ \pm 0.019^\circ$  and  $19.8065^\circ \pm 0.0006^\circ$ , showing that the comet will be leaving towards the Gemini constellation. The radial velocity of the comet will be  $58.01 \pm 0.01 \text{ km s}^{-1}$ . The corresponding Galactic longitude,  $l$ , will be  $191.943^\circ \pm 0.008^\circ$  and the Galactic latitude will be  $2.559^\circ \pm 0.016^\circ$ . The comet 3I will reach a distance of  $1221.41 \pm 0.25 \text{ au}$  from the Sun at the end of 100 years. The Ecliptic longitude ( $\lambda$ ) and the Ecliptic latitude ( $\beta$ ) will be  $95.011^\circ \pm 0.018^\circ$  and  $-3.541^\circ \pm 0.001^\circ$  respectively.

The future velocities in the ICRS frame,  $v_x$ ,  $v_y$  and  $v_z$ , are found to be  $-4.98 \pm 0.02 \text{ km s}^{-1}$ ,  $54.34 \pm 0.01 \text{ km s}^{-1}$  and  $19.65 \pm 0.01 \text{ km s}^{-1}$  which are converted into Galactic space velocities as described in the previous section. The galactic space velocities ( $U$ ,  $V$ ,  $W$ ) are  $(-56.70 \pm 0.01, -11.95 \pm 0.01, 2.51 \pm 0.02) \text{ km s}^{-1}$ . The solar motion corrected velocities are  $(67.80 \pm 0.69, 0.29 \pm 0.47, 9.76 \pm 0.36) \text{ km s}^{-1}$ .

#### 3.2.2. Short-term integration

As we can see in the Figure 1, there are possible close encounters with Mars and Jupiter on epochs JD 2460951.5 (2025 October 03) and JD 2461115.5 (2026 March 16), respectively. The minimum expected distance would be 0.19 au from Mars and 0.357 au from Jupiter. The distance of the comet 3I from Jupiter is

very close to the Hill radius (0.355 au) of Jupiter. Therefore, there could be a stronger perturbation from Jupiter compared to Mars.

In short-term integration, the comet nominal orbit and its statistical clones are integrated for twenty years using the highly precise mathematical integrator IAS15 with a time step of 1 hour. The variation of the orbital elements such as semi-major axis ( $a$ ), eccentricity ( $e$ ), inclination ( $i$ ), Longitude of Ascending Node ( $\Omega$ ), Argument of Periapsis ( $\omega$ ), and the cartesian velocities in the  $z$ -axis are shown in Figure 2 for two years. We also checked for post-Newtonian (General Relativistic) correction using the GR force from the REBOUNDX package (D. Tamayo et al. 2019) and didn't see any significant effects affecting the solutions.

In the plots, the gray color represents the orbital evolution of cometary clones in the absence of Mars and Jupiter, while the blue color curves represent the effect of both Mars and Jupiter. The vertical red and black dashed line represents the time of close approach with Mars and Jupiter. The vertical, indigo-dotted line represents the time of perihelion. As we can see, there is a strong effect on the orbital parameters, such as semi-major axis ( $a$ ), eccentricity ( $e$ ), inclination ( $i$ ), Longitude of Ascending Node ( $\Omega$ ), and Argument of Periapsis ( $\omega$ ), in the presence of Mars and Jupiter. Also, its  $z$ -axis velocity will be significantly perturbed due to the planetary interaction. The other parameters, namely, cartesian coordinates, i.e.,  $x$ ,  $y$ ,  $z$ , cartesian velocities,  $v_x$  and  $v_y$ , and the sixth orbital element, Mean Anomaly, are not significantly perturbed by the interaction.

Since there is a possibility of close observation from the Juno spacecraft using its suite of onboard instruments, we have considered a different simulation where the Juno spacecraft is added in REBOUND with IAS15 integrator. Taking the maximum distance from Juno to be 0.4 au for optimal observation, and the time at which the distance between comet 3I and the Juno spacecraft is less than the distance between comet 3I and Jupiter, we suggest that the optimal period for observation is from 09<sup>th</sup> to 22<sup>nd</sup> March 2026. The solar elongation angle (Sun-Juno-Comet angle) during this period will be between  $28^\circ$  to  $100^\circ$  as shown in Figure 3.

#### 3.2.3. Non-Gravitational Acceleration

The comets are subjected to non-gravitational acceleration due to outgassing, as mentioned in the introduction. The non-gravitational forces are defined as:

$$F_i = A_i g(r), i = 1, 2, 3 \quad (1)$$

where  $A_1$  is the non-gravitational acceleration in the radial direction,  $A_2$  in the transverse direction, and  $A_3$  in

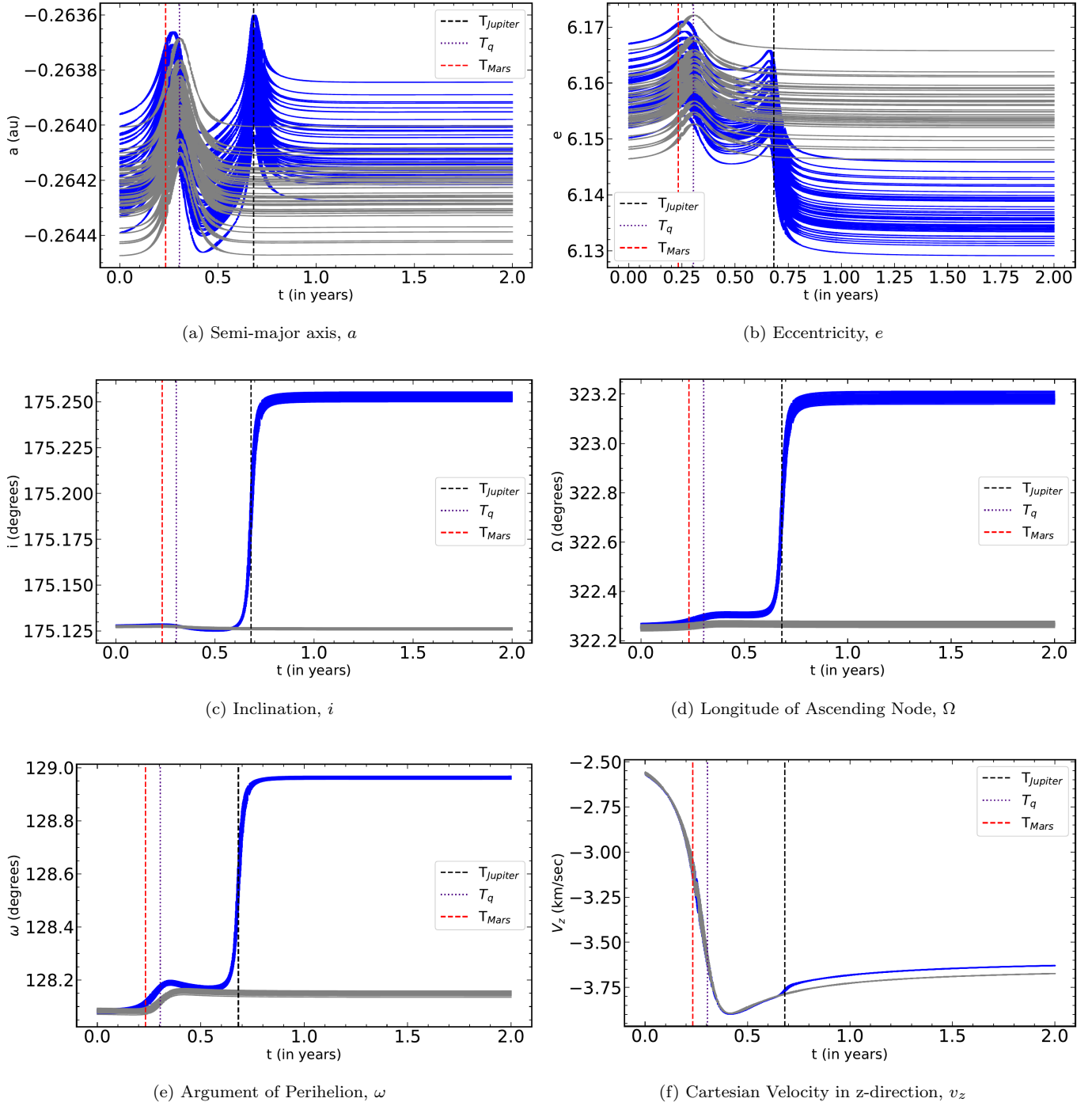


**Figure 2.** Variation of Orbital Parameters and the Cartesian velocity in z-direction. In each panel, the gray curves are for the simulation without considering interactions with Mars and Jupiter, whereas the blue curves include these planets. The vertical red and black dashed lines represent the date at which the comet is close to Mars and Jupiter. The vertical dotted lines in indigo represent the time of perihelion. Here, we plotted the behavior of 50 clones to keep the image size manageable.

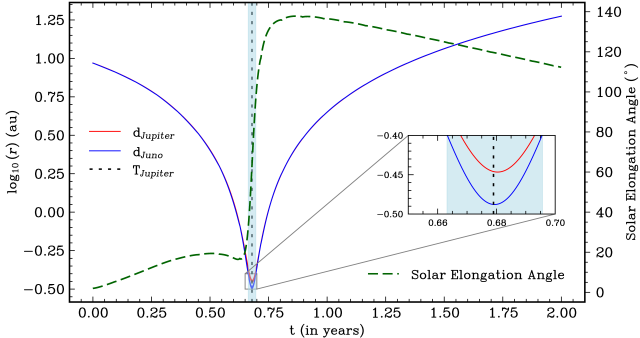


**Figure 3.** The distance from comet to Juno spacecraft,  $d_{Juno}$ , and Jupiter  $d_{Jupiter}$ , are plotted in blue and red curves respectively in log scale. The black dashed line is the time of the interaction with Jupiter. The masked region is for the optimal observation when the comet 3I will be at 0.4 au or below from the Juno spacecraft with a solar elongation between  $28^\circ$  to  $100^\circ$ .

the normal direction.  $g(r)$  is the semi-empirical function defined as:

$$g(r) = \alpha \left( \frac{r}{r_0} \right)^{-m} \left[ 1 + \left( \frac{r}{r_0} \right)^n \right]^{-k} \quad (2)$$

Here, different constants such as  $\alpha$ ,  $m$ ,  $n$ ,  $k$ ,  $r_0$  are taken from [M. Królikowska & P. A. Dybczyński \(2017\)](#). These parameters depend on the perihelion distance. If the perihelion distance is less than 4 au, which is true for the comet 3I, the values of constants will be  $\alpha = 0.1113$ ,  $m = 2.15$ ,  $n = 5.093$ ,  $k = 4.6142$ ,  $r_0 = 2.808$  au, representing the outgassing due to the water sublimation. For more details, see [B. G. Marsden et al. \(1973\)](#); [A. Sosa & J. A. Fernández \(2011\)](#); [M. Królikowska & P. A. Dybczyński \(2017\)](#). Therefore, to predict the effects of non-gravitational forces on comet 3I, we have included the non-gravitational accelerations in all three components in the simulation. There is another parameter called the DT (time offset in maximum brightness) parameter, representing the asymmetric cometary emission. Since it is difficult to constrain this in advance, we have not included it in our simulation.

As we write, we have verified that a new solution exists at the epoch JD 2460878.5 (2025-Jul-22.0) TDB; however, the non-gravitational accelerations remain unknown. Hence, we have used the Windows version of the `Find_Orb` software, as provided by [B. Gray \(2022\)](#), to fit the orbit and extract the non-gravitational accelerations. We utilize 3,997 observations (May 8 - September 29, 2025) from the Minor Planet Center (MPC) to predict non-gravitational accelerations in different components. We obtain a well-constrained and stable solution to the non-gravitational accelerations only when we consider a symmetric model of comet  $A_1$  and  $A_2$  pa-

rameters with  $A_3$  and DT parameters equal to zero. We find  $A_1$  is  $(1.5 \pm 0.2) \times 10^{-6}$  and  $A_2$  is  $(2.74 \pm 0.95) \times 10^{-6}$  respectively, having positive signs for both  $A_1$  and  $A_2$  components.

We rerun our simulations with different positive values of the non-gravitational accelerations in the  $A_1$  and  $A_2$  parameters, with values ranging from  $10^{-5}$  au day $^{-2}$  to  $10^{-9}$  au day $^{-2}$ .

We have plotted the results of the variation of the orbital elements semi-major axis ( $a$ ), eccentricity ( $e$ ), inclination ( $i$ ), Longitude of Ascending Node ( $\Omega$ ), Argument of Periapsis ( $\omega$ ), and the cartesian velocity in the  $z$ -axis in Figure 4. As seen in the Figure 4, the non-gravitational accelerations to show a significant effect on comet 3I are  $10^{-5}$  auday $^{-2}$ ,  $10^{-6}$  auday $^{-2}$ . The non-gravitational acceleration of  $10^{-7}$  auday $^{-2}$  shows a very small effect. The rest of the accelerations below  $10^{-7}$  auday $^{-2}$  show negligible variation from the results given by considering only the gravitational effects. For the strongest non-gravitational acceleration  $10^{-5}$  auday $^{-2}$ , the ICRS coordinates: RA ( $\alpha$ ) and Declination ( $\delta$ ) of the comet after 20 years when the comet reaches close to 250 au, are found to be  $96.218^\circ \pm 0.015^\circ$  and  $19.454^\circ \pm 0.0005^\circ$ . The Galactic space velocities ( $U, V, W$ ) are  $(-57.09 \pm 0.01, -12.63 \pm 0.01, 2.86 \pm 0.02)$  kms $^{-1}$ .

Similarly, for the non-gravitational acceleration of  $10^{-6}$  auday $^{-2}$ , the ICRS coordinates: RA ( $\alpha$ ) and Declination ( $\delta$ ) of the comet are found to be  $95.702^\circ \pm 0.015^\circ$  and  $19.774^\circ \pm 0.0005^\circ$ . The galactic space velocities ( $U, V, W$ ) are  $(-56.78 \pm 0.01, -12.03 \pm 0.01, 2.55 \pm 0.02)$  kms $^{-1}$ . For comparison, in the absence of non-gravitational accelerations, the ICRS coordinates: RA ( $\alpha$ ) and Declination ( $\delta$ ) of the comet after 20 years are found to be  $95.634^\circ \pm 0.015^\circ$  and  $19.8102^\circ \pm 0.0005^\circ$ . The galactic space velocities ( $U, V, W$ ) are  $(-56.74 \pm 0.01, -11.96 \pm 0.01, 2.51 \pm 0.01)$  kms $^{-1}$ .

We have also examined the variation in the Cartesian coordinates  $x$ , and  $z$ , as well as the Cartesian velocities  $v_x$  and  $v_y$ . There is no visible effect in the  $y$  coordinate. The major effect of the non-gravitational acceleration is seen for the values of  $10^{-5}$  auday $^{-2}$ , while the non-gravitational accelerations below  $10^{-5}$  auday $^{-2}$  have no significant effect (See Figure 6 in the appendix section A).

### 3.2.4. Comparing the distribution of clones with or without non-gravitational accelerations.

Since there could be a strong effect from Jupiter, we plotted the histogram of the distribution of the close approach distances of the cometary clones when they approach Jupiter. In the first case, we consider the effect of gravitational forces only. As shown in Figure 5a, the mean minimum distance for clones from Jupiter is

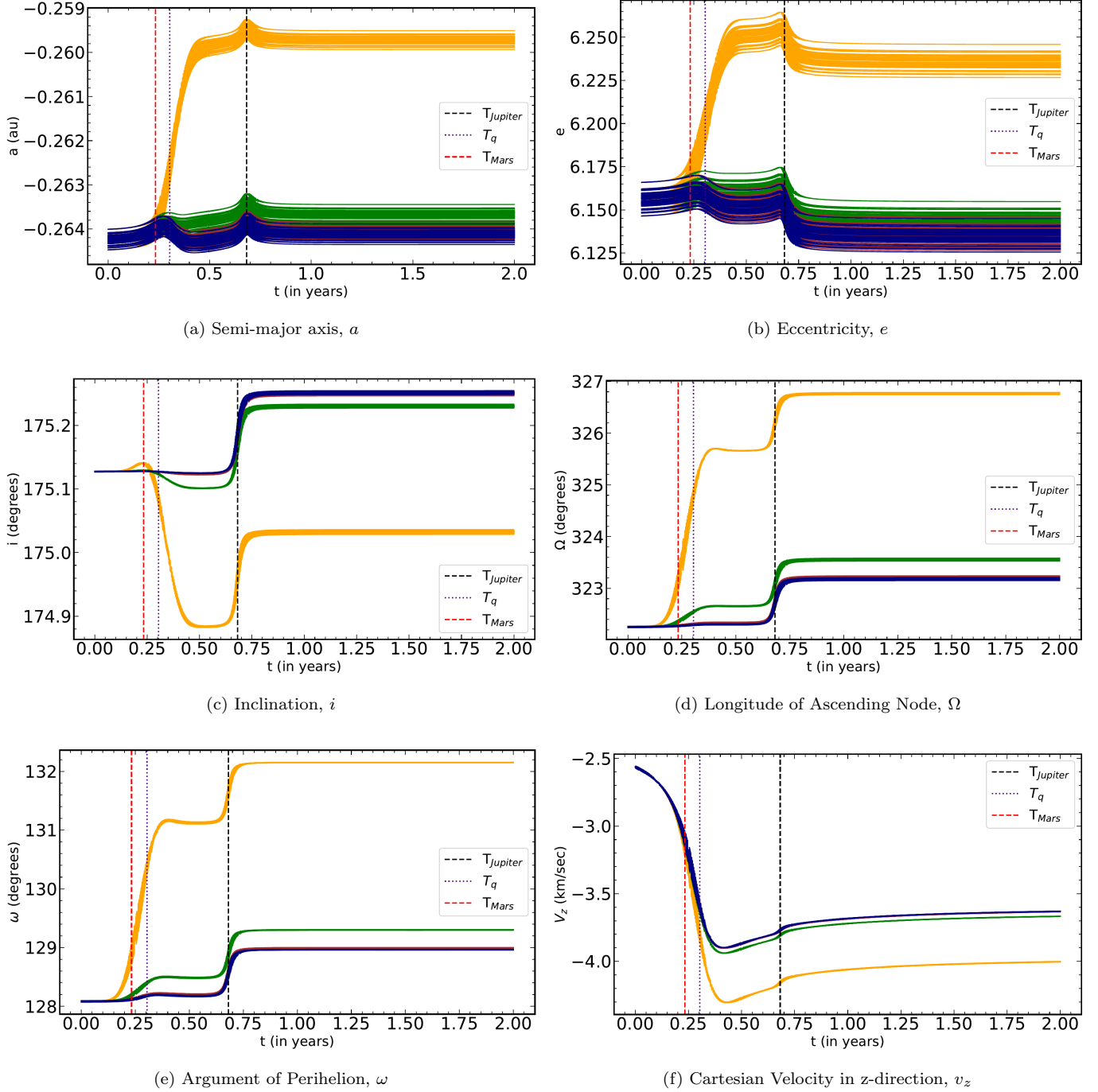
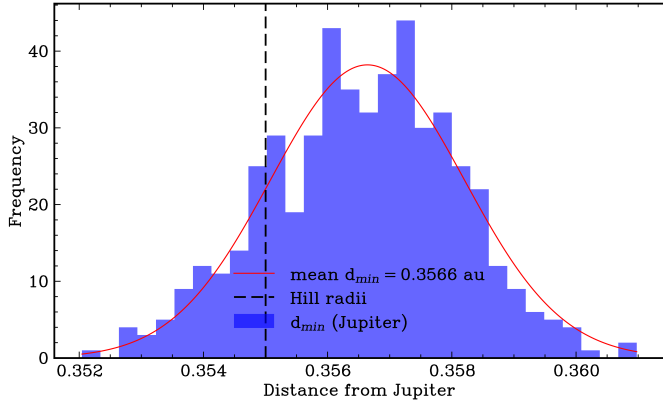
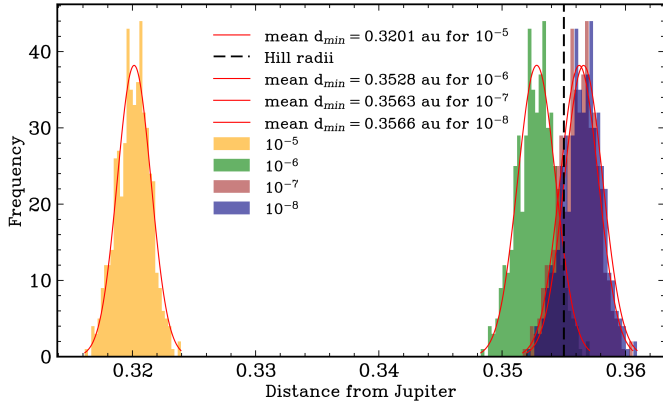


**Figure 4.** Variation of Orbital Parameters and the Cartesian velocity in z-direction. In each panel, the orange curves represent non - gravitational accelerations of  $10^{-5}$  auday $^{-2}$ , the green, brown and navy blue curves represent non - gravitational accelerations of  $10^{-6}$  auday $^{-2}$ ,  $10^{-7}$  auday $^{-2}$ , and  $10^{-8}$  auday $^{-2}$ . Here, we plotted the behavior of 50 clones to keep the image size manageable.



(a) Histogram of the minimum distance from Jupiter for simulations with 500 clones in the presence of gravitational forces only.



(b) Histogram of the minimum distance from Jupiter for simulations with 500 clones in the presence of both gravitational and non-gravitational forces. The different non-gravitational accelerations are marked in the same colours as the previous plots.

**Figure 5.** Histogram of 500 cometary clones in the presence of different forces.

0.3566 au with a  $1-\sigma$  of 0.0016 au. We find that 81 out of 500 clones pass at distances lesser than the Hill radius of Jupiter.

For different non-gravitational forces, the mean of the close-approach distance changes significantly, when we consider the non-gravitational acceleration of  $10^{-5}$   $\text{auday}^{-2}$ , the mean value of the minimum distance is 0.3201 and 100 % of clones are inside the Hill radius of Jupiter while for non-gravitational acceleration of  $10^{-6}$   $\text{auday}^{-2}$  470 out of 500 clones are inside the Hill radius of Jupiter with a mean value of 0.3528 (see Figure 5b). For non-gravitational acceleration of  $10^{-7}$   $\text{auday}^{-2}$ , 116 out of 500 clones are inside the Hill radius of Jupiter with a mean value of 0.3563, and for  $10^{-8}$   $\text{auday}^{-2}$ , 87 out of 500 clones are inside the Hill radius of Jupiter with a mean value of 0.3566.

#### 4. SUMMARY AND CONCLUSION

In this letter, we have studied the effects of both gravitational perturbations from Mars and Jupiter, as well as non-gravitational forces resulting from cometary emission, on comet 3I. We have found the following:

- The comet 3I will definitely suffer the perturbation from both Mars and Jupiter at their respective close approach epochs. The effect of Jupiter will be larger due to the fact that the comet is passing very close to the Hill radius of Jupiter.
- The long-term orbital integration of 500 statistical clones of comet 3I for hundred years in the past and future shows that the comet is coming from the Sagittarius constellation with a mean radial velocity of  $-57.995 \pm 0.011 \text{ km s}^{-1}$  and leaving towards the Gemini constellation with a mean radial velocity of  $58.01 \pm 0.01 \text{ km s}^{-1}$ .
- The solar motion corrected Galactic space velocities  $(U, V, W)$  at 1 hundred years ago are  $(62.36 \pm 0.69, -7.16 \pm 0.47, 26.18 \pm 0.36) \text{ km s}^{-1}$ . Correspondingly, the comet 3I's  $(U_{LSR}^2 + V_{LSR}^2 + W_{LSR}^2)^{1/2}$  is  $68.01 \pm 0.82 \text{ km s}^{-1}$ . From the Toomre diagram mentioned in the [M. P. da Silva et al. \(2023\)](#), we found that the comet total velocity,  $V_{Total}$ ,  $(U_{LSR}^2 + V_{LSR}^2 + W_{LSR}^2)^{1/2}$ , is between 50 to 70  $\text{km s}^{-1}$ . Hence, the possible location of the comet 3I is found to be in the transition zone from the thin to the thick disk. Therefore, it is uncertain to confirm the region of origin using kinematic information.
- The short-term orbital integration for 20 years in the presence of gravitational perturbation affects the various orbital parameters and Cartesian velocity in the z-axis significantly, as shown in Figure 2.
- A stable solution for the non-gravitational accelerations using `Find_Orb` has been derived when we consider the symmetric model. The non-gravitational accelerations,  $A_1$  and  $A_2$ , are found to be  $(1.5 \pm 0.2) \times 10^{-6}$  and  $(2.74 \pm 0.95) \times 10^{-6}$  respectively.
- The integration in the presence of non-gravitational forces can significantly affect the orbital parameters, resulting in a change in the future orbital evolution of the comet 3I, as shown in Figures 4 and 6. We find that the major effects on comet 3I's orbit are seen when the non-gravitational acceleration is of the order of  $10^{-5}$  to

$10^{-6}$  auday $^{-2}$ . The non-gravitational acceleration of  $10^{-7}$  auday $^{-2}$  and lower has negligible effect on the various parameters.

- The optimal window of the observation from the Juno spacecraft will be from 09<sup>th</sup> to 22<sup>nd</sup> March 2026. During this time, the solar elongation angle will be between 28° to 100°.
- Further observations of the comet 3I are required to confirm the non-gravitational accelerations. Additionally, if the light curve of comet 3I is asymmetric, then the DT (time offset in the maximum brightness) parameter will be crucial in calculating the effect of non-gravitational forces.

#### ACKNOWLEDGMENTS

We thank the anonymous reviewer for providing valuable comments and helpful suggestions. GA would like to thank Prof. Raul de la Fuente Marcos for the discussion on the Galactocentric coordinate system. We

would also like to thank Prof. Agnes Fienga for the discussion on the numerical simulation and useful suggestions. Work at the Physical Research Laboratory is supported by the Department of Space, Govt. of India. The computations were performed on the Param Vikram-1000 High Performance Computing Cluster of the Physical Research Laboratory (PRL).

#### AUTHOR CONTRIBUTIONS

GA: Conceptualization, Methodology, Software, Formal analysis, Visualization, Writing – original draft.

SG: Supervision, Writing – review & editing.

*Software:* Astropy ( Astropy Collaboration et al. 2013, 2018, 2022), Astroquery (A. Ginsburg et al. 2019), Numpy (C. R. Harris et al. 2020), Scipy (P. Virtanen et al. 2020), Matplotlib (J. D. Hunter 2007), Smplotlib (J. Li 2023), Pandas (T. pandas development team 2020), REBOUND (H. Rein & S. F. Liu 2012; H. Rein & D. S. Spiegel 2015), REBOUNDX (D. Tamayo et al. 2019), Find\_Orb (B. Gray 2022)

#### APPENDIX

#### A. VARIATION OF DIFFERENT PARAMETERS CONSIDERING NON-GRAVITATIONAL SOLUTION

Here, we show the variation of the Cartesian coordinates, i.e.,  $x$ , and  $z$ , and the Cartesian velocities in the x-direction,  $v_x$ , and the y-direction,  $v_y$ , of 50 statistical clones (for representation purposes only) for two years under the influence of both gravitational and non-gravitational forces.

#### REFERENCES

Anderson, S., Rousselot, P., Jehin, E., et al. 2024, in European Planetary Science Congress, EPSC2024-59, doi: [10.5194/epsc2024-59](https://doi.org/10.5194/epsc2024-59)

Anderson, S. E., Rousselot, P., Noyelles, B., Jehin, E., & Mousis, O. 2023, Monthly Notices of the Royal Astronomical Society, 524, 5182, doi: [10.1093/mnras/stad2092](https://doi.org/10.1093/mnras/stad2092)

Aravind, K., Ganesh, S., Venkataramani, K., et al. 2021, Monthly Notices of the Royal Astronomical Society, 502, 3491, doi: [10.1093/mnras/stab084](https://doi.org/10.1093/mnras/stab084)

Astropy Collaboration, Robitaille, T. P., Tollerud, E. J., et al. 2013, A&A, 558, A33, doi: [10.1051/0004-6361/201322068](https://doi.org/10.1051/0004-6361/201322068)

Astropy Collaboration, Price-Whelan, A. M., Sipőcz, B. M., et al. 2018, AJ, 156, 123, doi: [10.3847/1538-3881/aabc4f](https://doi.org/10.3847/1538-3881/aabc4f)

Astropy Collaboration, Price-Whelan, A. M., Lim, P. L., et al. 2022, ApJ, 935, 167, doi: [10.3847/1538-4357/ac7c74](https://doi.org/10.3847/1538-4357/ac7c74)

Bensby, T., Feltzing, S., & Lundström, I. 2003, A&A, 410, 527, doi: [10.1051/0004-6361:20031213](https://doi.org/10.1051/0004-6361:20031213)

Bodewits, D., Noonan, J. W., Feldman, P. D., et al. 2020, Nature Astronomy, 4, 867, doi: [10.1038/s41550-020-1095-2](https://doi.org/10.1038/s41550-020-1095-2)

Bolin, B. T., Belyakov, M., Fremling, C., et al. 2025, Monthly Notices of the Royal Astronomical Society: Letters, slaf078, doi: [10.1093/mnrasl/slaf078](https://doi.org/10.1093/mnrasl/slaf078)

da Silva, M. P., Alves-Brito, A., & do Nascimento, J D, J. 2023, Monthly Notices of the Royal Astronomical Society, 527, 11082, doi: [10.1093/mnras/stad3937](https://doi.org/10.1093/mnras/stad3937)

de la Fuente Marcos, C., & de la Fuente Marcos, R. 2012, Monthly Notices of the Royal Astronomical Society, 427, 728, doi: [10.1111/j.1365-2966.2012.21936.x](https://doi.org/10.1111/j.1365-2966.2012.21936.x)

de la Fuente Marcos, C., & de la Fuente Marcos, R. 2014, Monthly Notices of the Royal Astronomical Society, 439, 2970, doi: [10.1093/mnras/stu152](https://doi.org/10.1093/mnras/stu152)

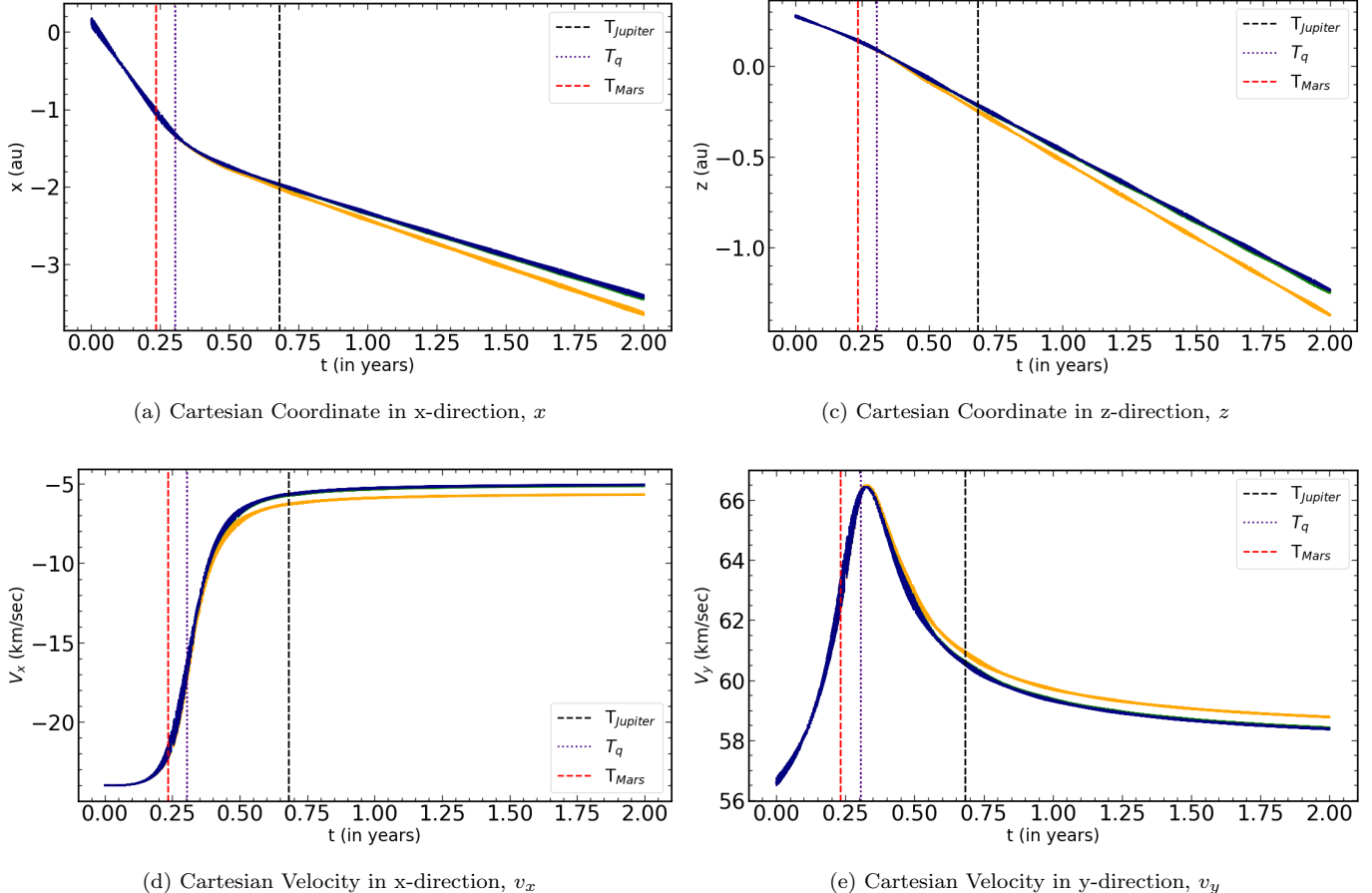


**Figure 6.** Variation of Cartesian Coordinates,  $x$ , and  $z$ , the Cartesian velocities,  $v_x$ , and  $v_y$ . In each panel, the orange curves represent non - gravitational accelerations of  $10^{-5}$  auday $^{-2}$ , the green, brown and navy blue curves represent non - gravitational accelerations of  $10^{-6}$  auday $^{-2}$ ,  $10^{-7}$  auday $^{-2}$ , and  $10^{-8}$  auday $^{-2}$ . Here, we plotted the behavior of 50 clones to keep the image size manageable.

de la Fuente Marcos, R., Alarcon, M. R., Licandro, J., et al. 2025, A&A, 700, L9, doi: [10.1051/0004-6361/202556439](https://doi.org/10.1051/0004-6361/202556439)

Dybczyński, P. A., & Królikowska, M. 2011, Monthly Notices of the Royal Astronomical Society, 416, 51, doi: [10.1111/j.1365-2966.2011.19005.x](https://doi.org/10.1111/j.1365-2966.2011.19005.x)

Egal, A., Wiegert, P., & Brown, P. G. 2022, Monthly Notices of the Royal Astronomical Society, 515, 2800, doi: [10.1093/mnras/stac1839](https://doi.org/10.1093/mnras/stac1839)

Fitzsimmons, A., Hainaut, O., Meech, K. J., et al. 2019, ApJL, 885, L9, doi: [10.3847/2041-8213/ab49fc](https://doi.org/10.3847/2041-8213/ab49fc)

Gabryszewski, R., Wajer, P., & Włodarczyk, I. 2024, A&A, 691, A130, doi: [10.1051/0004-6361/202347278](https://doi.org/10.1051/0004-6361/202347278)

Ginsburg, A., Sipócz, B. M., Brasseur, C. E., et al. 2019, AJ, 157, 98, doi: [10.3847/1538-3881/aafc33](https://doi.org/10.3847/1538-3881/aafc33)

Giorgini, J. D., Yeomans, D. K., Chamberlin, A. B., et al. 1996, in AAS/Division for Planetary Sciences Meeting Abstracts, Vol. 28, AAS/Division for Planetary Sciences Meeting Abstracts #28, 25.04

Gray, B. 2022, Find\_Orb: Orbit determination from observations,, Astrophysics Source Code Library, record ascl:2202.016 <http://ascl.net/2202.016>

Guzik, P., Drahus, M., Rusek, K., et al. 2020, Nature Astronomy, 4, 53, doi: [10.1038/s41550-019-0931-8](https://doi.org/10.1038/s41550-019-0931-8)

Harris, C. R., Millman, K. J., van der Walt, S. J., et al. 2020, Nature, 585, 357, doi: [10.1038/s41586-020-2649-2](https://doi.org/10.1038/s41586-020-2649-2)

Hopkins, M. J., Dorsey, R. C., Forbes, J. C., et al. 2025, ApJL, 990, L30, doi: [10.3847/2041-8213/adfbf4](https://doi.org/10.3847/2041-8213/adfbf4)

Hui, M.-T., & Jewitt, D. 2017, The Astronomical Journal, 153, 80, doi: [10.3847/1538-3881/153/2/80](https://doi.org/10.3847/1538-3881/153/2/80)

Hunter, J. D. 2007, Computing in Science & Engineering, 9, 90, doi: [10.1109/MCSE.2007.55](https://doi.org/10.1109/MCSE.2007.55)

Jewitt, D., Hui, M.-T., Kim, Y., et al. 2020, The Astrophysical Journal Letters, 888, L23, doi: [10.3847/2041-8213/ab621b](https://doi.org/10.3847/2041-8213/ab621b)

Jewitt, D., & Seligman, D. Z. 2023, ARA&A, 61, 197, doi: [10.1146/annurev-astro-071221-054221](https://doi.org/10.1146/annurev-astro-071221-054221)

Johnson, D. R. H., & Soderblom, D. R. 1987, AJ, 93, 864, doi: [10.1086/114370](https://doi.org/10.1086/114370)

Królikowska, M., & Dybczyński, P. A. 2010, Monthly Notices of the Royal Astronomical Society, 404, 1886, doi: [10.1111/j.1365-2966.2010.16403.x](https://doi.org/10.1111/j.1365-2966.2010.16403.x)

Królikowska, M., & Dybczyński, P. A. 2017, Monthly Notices of the Royal Astronomical Society, 472, 4634, doi: [10.1093/mnras/stx2157](https://doi.org/10.1093/mnras/stx2157)

Li, J. 2023, AstroJacobLi/smplotlib: v0.0.9, v0.0.9 Zenodo, doi: [10.5281/zenodo.8126529](https://doi.org/10.5281/zenodo.8126529)

Marsden, B. G., Sekanina, Z., & Yeomans, D. K. 1973, AJ, 78, 211, doi: [10.1086/111402](https://doi.org/10.1086/111402)

Meech, K. J., Weryk, R., Micheli, M., et al. 2017, Nature, 552, 378, doi: [10.1038/nature25020](https://doi.org/10.1038/nature25020)

Micheli, M., Farnocchia, D., Meech, K. J., et al. 2018, Nature, 559, 223, doi: [10.1038/s41586-018-0254-4](https://doi.org/10.1038/s41586-018-0254-4)

Opitom, C., Fitzsimmons, A., Jehin, E., et al. 2019, A&A, 631, L8, doi: [10.1051/0004-6361/201936959](https://doi.org/10.1051/0004-6361/201936959)

Oumuamua ISSI Team, Bannister, M. T., Bhandare, A., et al. 2019, Nature Astronomy, 3, 594, doi: [10.1038/s41550-019-0816-x](https://doi.org/10.1038/s41550-019-0816-x)

pandas development team, T. 2020, pandas-dev/pandas: Pandas, 2.2.3 Zenodo, doi: [10.5281/zenodo.3509134](https://doi.org/10.5281/zenodo.3509134)

Pilorz, S., & Jenniskens, P. 2025, Icarus, 437, 116559, doi: <https://doi.org/10.1016/j.icarus.2025.116559>

Prodan, G. P., Popescu, M., Licandro, J., et al. 2024, Monthly Notices of the Royal Astronomical Society, 529, 3521, doi: [10.1093/mnras/stae539](https://doi.org/10.1093/mnras/stae539)

Rein, H., & Liu, S. F. 2012, A&A, 537, A128, doi: [10.1051/0004-6361/201118085](https://doi.org/10.1051/0004-6361/201118085)

Rein, H., & Spiegel, D. S. 2015, MNRAS, 446, 1424, doi: [10.1093/mnras/stu2164](https://doi.org/10.1093/mnras/stu2164)

Schönrich, R., Binney, J., & Dehnen, W. 2010, MNRAS, 403, 1829, doi: [10.1111/j.1365-2966.2010.16253.x](https://doi.org/10.1111/j.1365-2966.2010.16253.x)

Seligman, D. Z., Micheli, M., Farnocchia, D., et al. 2025, ApJL, 989, L36, doi: [10.3847/2041-8213/adf49a](https://doi.org/10.3847/2041-8213/adf49a)

Shober, P. M., Tancredi, G., Vaubaillon, J., et al. 2024, A&A, 687, A181, doi: [10.1051/0004-6361/202449635](https://doi.org/10.1051/0004-6361/202449635)

Sosa, A., & Fernández, J. A. 2011, Monthly Notices of the Royal Astronomical Society, 416, 767, doi: [10.1111/j.1365-2966.2011.19111.x](https://doi.org/10.1111/j.1365-2966.2011.19111.x)

Tamayo, D., Rein, H., Shi, P., & Hernandez, D. M. 2019, Monthly Notices of the Royal Astronomical Society, 491, 2885, doi: [10.1093/mnras/stz2870](https://doi.org/10.1093/mnras/stz2870)

Virtanen, P., Gommers, R., Oliphant, T. E., et al. 2020, Nature Methods, 17, 261, doi: [10.1038/s41592-019-0686-2](https://doi.org/10.1038/s41592-019-0686-2)

Ye, Q.-Z., Zhang, Q., Kelley, M. S. P., & Brown, P. G. 2017, ApJL, 851, L5, doi: [10.3847/2041-8213/aa9a34](https://doi.org/10.3847/2041-8213/aa9a34)